



ORIGINAL ARTICLE

The effects of feedback on stability and maneuverability of a phase-reduced model for cockroach locomotion

J. L. Proctor¹ · P. Holmes²

Received: 29 March 2017 / Accepted: 5 June 2018 / Published online: 15 June 2018
© Springer-Verlag GmbH Germany, part of Springer Nature 2018

Abstract

In previous work, we built a neuromechanical model for insect locomotion in the horizontal plane, containing a central pattern generator, motoneurons, muscles actuating jointed legs, and rudimentary proprioceptive feedback. This was subsequently simplified to a set of 24 phase oscillators describing motoneuronal activation of agonist–antagonist muscle pairs, which facilitates analyses and enables simulations over multi-dimensional parameter spaces. Here we use the phase-reduced model to study dynamics and stability over the typical speed range of the cockroach *Blaberus discoidalis*, the effects of feedback on response to perturbations, strategies for turning, and a trade-off between stability and maneuverability. We also compare model behavior with experiments on lateral perturbations, changes in body mass and moment of inertia, and climbing dynamics, and we present a simple control strategy for steering using exteroceptive feedback.

Keywords Exteroception · Feedback control · Hybrid systems · Neuromechanics · Proprioception · Stability–maneuverability trade-off

1 Introduction

Animals are adept at traversing complicated terrain. Insects, in particular, use their hexapedal gaits to run nimbly, maneuver, forage, and escape. Their abilities have inspired experimental studies, the development of mathematical models (Holmes et al. 2006), and the creation of legged robots (Altendorfer et al. 2001; Delcomyn 2004). Experiments on cockroaches and models of them have been especially revealing (e.g., Full and Tu 1991; Ting et al. 1994; Kubow and Full 1999; Full and Koditschek 1999; Full et al. 2002; Schmitt et al. 2002), demonstrating that feedforward activation of the body–limb mechanics suffices for stable running and provides rapid recovery from large impulsive perturbations (Jindrich and Full 2002; Kukillaya and Holmes 2007, 2009). However,

it is known that reflexive feedback can modify motoneuron spike (action potential) timing and numbers in a burst, while running fast over rough terrain (Sponberg and Full 2008). This implies a subtle combination of feedforward and feedback strategies, motivating further experiments and theoretical studies.

The present paper builds on work including that cited above, and a series of studies of the central pattern generator (CPG) and proprioceptive feedback in cockroaches (Pearson and Iles 1970, 1971; Pearson 1972; Pearson and Iles 1973; Delcomyn 1980; Zill and Moran 1981a; Zill et al. 1981; Zill and Moran 1981b), more recently supplemented by Fuchs et al. (2011, 2012) and David et al. (2016). These have led to a range of increasingly complex and realistic models of cockroach dynamics in the ground plane (Schmitt and Holmes 2000, 2003; Seipel et al. 2004; Ghigliazza and Holmes 2004a; Kukillaya and Holmes 2007, 2009), culminating in a neuromechanical system comprising CPG, nonlinear muscles actuating jointed legs, and proprioception from leg force sensors (Kukillaya et al. 2009). But with almost 300 ordinary differential equations (ODEs), this model is slow to simulate, impossible to analyze, and provides little insight on how its components interact. Phase reduction and averaging theory subsequently allowed us to replace 288 ODEs describing bursting interneurons, synaptic connections to motoneurons

Communicated by J. Leo van Hemmen.

✉ P. Holmes
pholmes@math.princeton.edu

¹ Institute for Disease Modeling, 3150, 139th Ave SE, Bellevue, WA 98005, USA

² Department of Mechanical and Aerospace Engineering, Program in Applied and Computational Mathematics and Princeton Neuroscience Institute, Princeton University, Princeton, NJ 08544, USA

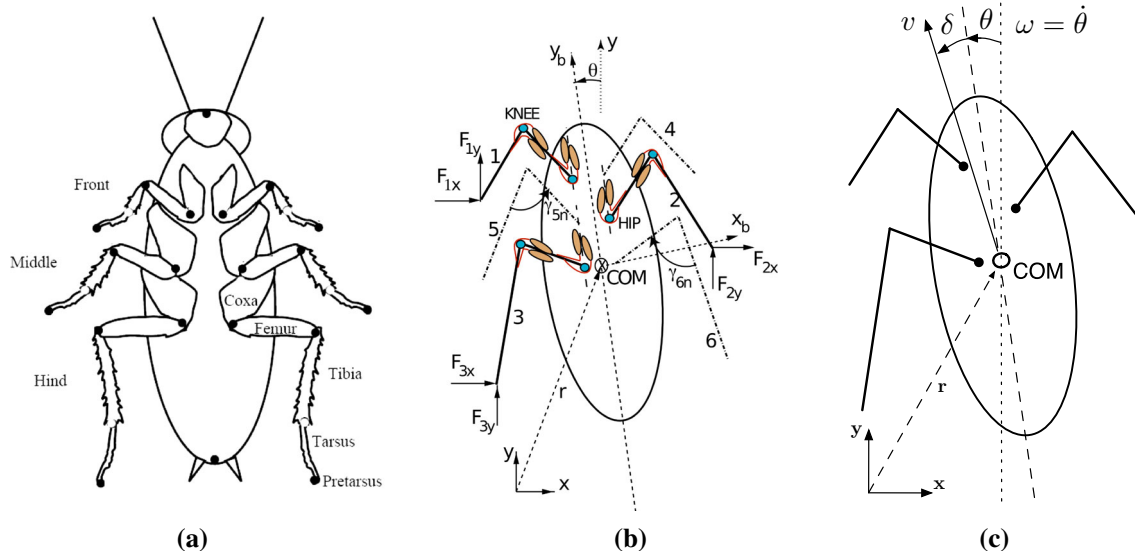


Fig. 1 **a** Ventral view of the cockroach *Blaberus discoidalis*, showing leg components; adapted from Kram et al. (1997, Fig. 1). **b** Dorsal view of the hexapedal model with pairs of Hill-type muscles actuating each joint; solid and dotted lines denote stance and swing legs; inertial frame

(x, y) and body frame (x_b, y_b) coordinates are also shown. **c** State space variables of the Poincaré map (5). Adapted from Kukillaya and Holmes (2009) and Kukillaya et al. (2009)

(MNs), muscle activation dynamics, and force-sensing neurons, with 24 phase oscillators modeling MNs in Proctor et al. (2010). [This was later reduced to a 6-oscillator model which was fitted to free running data from cockroaches (Couzin-Fuchs et al. 2015).]

In the present paper, we use the 24-oscillator model to further investigate the role of reflexive feedback, and its effects on turning and maneuverability. We maintain close ties to biological observations, using data from *Blaberus discoidalis* as in previous work. In Sect. 2, we review the model and describe its key features. New work begins in Sect. 3 where we verify that the model runs stably over the speed range of *B. discoidalis* without feedback. In Sect. 4, we study the effect of proprioceptive feedback on the model's response to impulses and describe its turning performance with and without proprioception. Section 5 compares model behavior with recent experiments on lateral perturbations and the effects of added mass and moment of inertia, discusses climbing behavior, and presents a linearized control strategy for steering, using exteroceptive feedback. A discussion ensues in Sect. 6.

2 The neuromechanical model

The phase-reduced model of Proctor et al. (2010) is a direct descendent of passive bipedal (Schmitt and Holmes 2000) and actuated hexapedal mechanical models (Seipel et al. 2004; Kukillaya and Holmes 2007), the muscle-actuated hexapod of Kukillaya and Holmes (2009), and

the CPG-motoneuron model of Ghigliazza and Holmes (2004a), as integrated in Kukillaya et al. (2009). Here we briefly review the model, first describing its biomechanical components, then the CPG and its phase reduction, and finally the incorporation of proprioceptive feedback into the phase-reduced model. Further details, including parameter values and MATLAB codes, can be found in Electronic Physics Auxiliary Publication Service (2009) and Proctor et al. (2010) and its supplementary materials. The MATLAB codes used in the present work are available at GitHub: <https://github.com/joshlproctor/Phase-Reduced-Insect-Locomotion>.

2.1 Biomechanics: limb geometry, muscles, and neural activation

Cockroaches employ a double-tripod gait over a wide speed range (Full and Tu 1991). The left front and hind legs and the right middle leg support the body during the “left” stance phase, while the other legs leave the ground in a swing phase. Right stances and left swings are defined analogously. As in earlier work, we assume a 50% duty cycle: each tripod's touchdown (TD) coincides with liftoff (LO) of the contralateral (swing) tripod. Figures 1a, b illustrate the animal's body-limb geometry and its simplification to a rigid body retaining only two joints in each leg. Leg masses are neglected and dynamics considered in the horizontal plane, ignoring vertical motions, pitch, and roll. The body has three mechanical degrees of freedom (planar translations and yaw).

Written in inertial coordinates $\mathbf{r} = x\hat{\mathbf{i}} + y\hat{\mathbf{j}}$, the equations of motion are:

$$m\ddot{x} = \sum_i F_{ix}(\mathbf{r}_{fi} - \mathbf{r}, \theta, t), \tag{1}$$

$$m\ddot{y} = \sum_i F_{iy}(\mathbf{r}_{fi} - \mathbf{r}, \theta, t), \tag{2}$$

$$I\ddot{\theta} = \sum_i (\mathbf{r}_{fi} - \mathbf{r}) \times \mathbf{F}_i(\mathbf{r}_{fi} - \mathbf{r}, \theta, t), \tag{3}$$

where m and I are the body mass and yaw moment of inertia, $\mathbf{F}_i = F_{ix}\hat{\mathbf{i}} + F_{iy}\hat{\mathbf{j}}$ denotes the reaction force at foot i , the vectors \mathbf{r}_{fi} identify the TD foot positions (fixed in inertial space throughout each stance phase), and the sums run over $i = 1, 2, 3$ for L tripod and $i = 4, 5, 6$ for R tripod. The forces \mathbf{F}_i include passive, linear, joint stiffnesses, and damping, and are obtained from joint torques via the nonlinear leg kinematics.

The contributions of muscle forces to joint torques are determined by a Hill-type model (Hill 1938), described in §2 and Figs 1 and 2 of Kukillaya and Holmes (2009):

$$F_{\text{muscle}}(t) = F_0 a(t) F_L(l_m) F_V(v_m), \tag{4}$$

where $a(t)$ is an activation function modeling calcium release following the arrival of spikes from motoneurons, taken from Kukillaya and Holmes (2009, §2.1). The functions F_L and F_V describing force dependence on muscle length and velocity are fitted to experiments (Ahn and Full 2002; Ahn et al. 2006). To match observed foot forces from Ting et al. (1994), the scale factor F_0 is adjusted, along with stereotypical spike inputs, for each muscle pair, using the inverse fitting procedure of Kukillaya and Holmes (2009, §§3-4). Eqs. (1–4) form a feedforward, nonlinear, time-dependent, hybrid dynamical system, since the L and R tripods alternate in stance, cf. Guckenheimer and Johnson (1995).

As noted in Schmitt and Holmes (2000), the dynamics is invariant under planar translations, implying that the system state at TD of each tripod may be specified by four variables: center of mass (CoM) velocity magnitude v , velocity direction δ relative to the major body axis, body axis angle θ , and angular velocity $\omega = \dot{\theta}$: Fig. 1c. The dynamics are described by a 4-dimensional Left-TD to Left-TD Poincaré map (Guckenheimer and Holmes 2002; Holmes et al. 2006):

$$(v, \delta, \theta, \omega) \mapsto P(v, \delta, \theta, \omega). \tag{5}$$

Appropriately parameterized, the linearized model possesses a branch of gaits with one unit eigenvalue corresponding to body orientation. The other three eigenvalues generally lie within the unit circle, indicating partial asymptotic stability (Holmes et al. 2006), and supporting the proposal of Brown et al. (1995) that mechanical “preflexes” are primarily responsible for stability in rapid running.

2.2 The CPG, motoneurons and proprioceptive feedback

We now describe how the biomechanical model is driven. The cockroach CPG is located within the thorax, in three pairs of hemisegments, each innervating the muscles driving a corresponding leg. Little is known regarding cell types or neural architecture, but earlier work (Pearson and Iles 1970, 1971; Pearson 1972; Pearson and Iles 1973) established the presence of bursting interneurons that inhibit depressor motoneurons and excite levitator motoneurons in each hemisegment, and found evidence of inhibitory ipsilateral intersegmental connections. This work motivated ion-channel models of bursting neurons (Ghigliazza and Holmes 2004b) and the CPG network of Fig. 2a that was developed in Ghigliazza and Holmes (2004a, §§2-4). More recent studies (Fuchs et al. 2011, 2012) have reinforced this picture and provided estimates of ipsi- and contralateral coupling strengths, showing that the former are stronger in the descending (rostro-caudal) direction than ascending [unlike the rostro-caudally symmetric network of Ghigliazza and Holmes (2004a)]. Internal coupling is nonetheless weak (Fuchs et al. 2011), although the variability of the tripod-like phase relations among hemisegments is reduced by proprioceptive feedback from stepping legs (Fuchs et al. 2012).

Each of the six CPG units of Fig. 2a represents a pool of interneurons, and given identical parameters and hence bursting frequencies, they collectively produce a double-tripod rhythm. Units 1, 2 and 3 burst in phase, and 4, 5 and 6 likewise, in antiphase with 1, 2 and 3. The network therefore acts as a clock to set the stepping frequency by emitting two equi-spaced bursts of spikes per cycle to MNs associated with the left and right tripods. To actuate hip and knee joints in the model of Fig. 1b, each CPG unit drives two extensor and flexor pairs of fast MNs, which, respectively, excite and inhibit flexors and extensors in the simplified musculature of our horizontal plane model.

2.3 Phase reduction

For the models described above, weak coupling, phase response curves and averaging theory allow the 3-variable ODE describing each bursting unit, and the scalar ODE for its synaptic dynamics, to be reduced to a rotator or phase oscillator, characterized by a single angular variable ϕ_i (Holmes et al. 2006; Ghigliazza and Holmes 2004a). Letting i denote a CPG unit and j one of its associated MNs, the phase angle of the latter evolves as follows:

$$\dot{\phi}_j = \omega_0 + \epsilon [\delta_j + Z_j(\phi_j) g_{ij}(\phi_j, \phi_i, t)], \tag{6}$$

where the CPG ϕ_i has frequency ω_0 and the MN $\omega_0 + \epsilon \delta_j$. The phase response curve (PRC) $Z(\phi_j)$ describes the MN’s

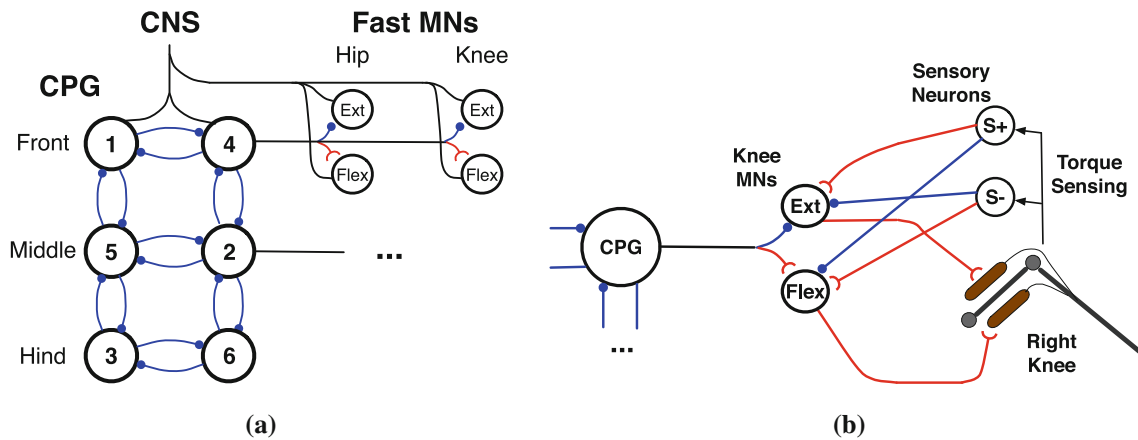


Fig. 2 a The CPG and motoneuron (MN) model. Units 1, 2, 3 (left tripod) and 4, 5, 6 (right tripod) are coupled through mutually inhibitory synapses and modulate each leg's hip and knee extensor (resp. flexor) motoneurons via inhibitory (resp. excitatory) synapses. Inhibitory synapses shown as filled circles; excitatory synapses as semi-arcs; only right front leg motoneurons shown here. Tonic drive is applied to all units via the central nervous system (CNS). See Ghigliazza and

Holmes (2004a, §§2–4) for further details. **b** Proprioceptive sensory feedback circuit. Positive and negative knee-joint torques are sensed by neurons $s+$ and $s-$, representing campaniform sensilla, that respectively excite and inhibit MNs innervating extensor and flexor muscles. One right knee circuit is shown, other legs are similar; synapses indicated as in **a**

receptivity to inputs g_{ij} , which may include feedback as well as periodic input from the CPG. (Proprioceptive feedback is discussed in Sect. 2.4.) Without feedback, Eq. (6) can be rewritten in terms of slowly varying phases $\psi_j = \phi_j - \omega_0 t$ and averaged over a cycle to yield:

$$\dot{\psi}_j = \epsilon \delta_j + \frac{\epsilon}{2\pi} \int_0^{2\pi} Z_j(\tau) g_{ij}(\tau, \psi_j - \psi_i + \tau) d\tau, \quad (7)$$

$$\stackrel{\text{def}}{=} G_{ij}(\psi_j - \psi_i), \quad (8)$$

where $\tau = \psi_j + \omega_0 t$ [see Guckenheimer and Holmes (2002, §§4.1–2) for the averaging theory of ODEs and Ghigliazza and Holmes (2004a, §5) and Proctor et al. (2010, §3) for details of the phase oscillator case]. The periodic coupling function G_{ij} , which depends only on the difference $\psi_j - \psi_i$, governs the phase relationship between the CPG and motoneuron and hence determines fixed points, eigenvalues, sensitivity of fixed points to the frequency difference $\epsilon \delta_j$, and entrainment ranges (Proctor and Holmes 2010).

The current model excludes proprioceptive and other time-dependent inputs to the CPG, so its 6 units run periodically, sending identical outputs to the left (L) and right (R) tripods with a half cycle (π) phase difference. This enforces contralateral reflection symmetry $\phi_1 = \phi_2 = \phi_3 \equiv \phi_L(t)$; $\phi_4 = \phi_5 = \phi_6 \equiv \phi_R(t)$ with a phase shift. Absent perturbations to and feedback from the legs, it produces a stereotypical double-tripod gait. We may further reduce to a pair of oscillators which then collapse to a single ODE for the phase difference $\theta = \phi_L - \phi_R$ between the L and R tripods:

$$\dot{\theta} = \mathcal{G}(\theta). \quad (9)$$

The coupling function $\mathcal{G}(\theta)$ resembles $\sin \theta$ (Ghigliazza and Holmes 2004a, Fig. 8), so that $\theta = \pi$ is a stable fixed point. Since no time-dependent inputs enter it, the CPG maintains frequency ω_0 and we can replace the individual CPG unit phases ψ_i in Eq. (8) by $\omega_0 t$ and $\omega_0 t + \pi$, describing a unique double-tripod gait.

Laborious tuning of the bursting MNs was required to find spike sequences that produced the experimentally derived foot forces of Ting et al. (1994). Briefly, Eqs. (1–3) and the leg geometry were used to find body kinematics and thence to compute periodic orbits over a range of stride frequencies. From this data, appropriate joint angles and torques, and hence muscle forces, were derived. MN spike sequences consistent with these forces were then found by running simulations of the CPG and biomechanical model in combination with an optimization algorithm that used the Matlab routine `lsqnonlin`. This iteratively improved and finally delivered spike numbers and inter-spike intervals for input to each muscle in the neuromechanical model of Kukillaya et al. (2009). Hand selection of initial spike data was required for the optimization algorithm. See Kukillaya and Holmes (2009, §4 and Figs. 4–9) for details.

Phase oscillators produce no spikes *per se*, so in Proctor et al. (2010) and the present work, analytical activation functions $a(t)$ representing calcium release at the neuromuscular junction, calculated as in Kukillaya and Holmes (2009, supplementary materials S1) from the spike sequences found above, are input to muscles as their MNs pass appropriate phase values. This simpler phase-reduced setting allows better understanding of phase ranges in which stable MN entrainment is possible, cf. Proctor et al. (2010).

2.4 Proprioceptive feedback of joint torques

Proximal and distal campaniform sensilla, located in the insect’s exoskeleton, independently detect bending of leg segments in opposing directions, and neurons within them fire tonically at rates approximately proportional to force magnitude (Zill and Moran 1981a; Zill et al. 1981; Zill and Moran 1981b). As in Proctor et al (2010, §2d), we neglect detailed mechanisms (cf. Kukillaya et al. 2009; Proctor and Holmes 2010) and assume that synaptic inputs to the MNs are determined by joint torques τ_{\pm} via the linear firing rate relationship

$$s_{\pm}(t) = b + n |\tau_{\pm}|, \tag{10}$$

with baseline level b and constant of proportionality n . Here \pm denotes the torque’s sense, positive meaning that extensor force exceeds flexor force, tending to extend the leg, and vice versa. Separate positive and negative sensors are allocated to each joint, and they are assumed to act only during stance while the leg exerts force on the body. (Swing phases of the massless legs are not modeled; hence, their effects are necessarily ignored.) The spike trains are relayed, via excitatory and inhibitory synapses, to extensor and flexor MNs activating the muscles of the joint in question, so that increased resistance to leg extension is compensated by increased joint torque and vice versa. As in Kukillaya et al. (2009) and Proctor et al. (2010), we model feedback from knee joints alone and include only direct paths from each joint to the MNs actuating it: see Fig. 2b. Sensory feedback of joint torques is included only for the simulations of §4.

2.5 The phase-reduced CPG-MN model

The phase-reduced model is shown schematically in Fig. 3, excluding the torque-sensing circuits from the six knee joints, each of which is as in Fig. 2b. The 6 oscillators of Fig. 2a are replaced by a single CPG “clock” running at $\omega_0/(2\pi)$ Hz, outputting the periodic spike sequences from Kukillaya and Holmes (2009) to drive the 24 MNs in a feedforward manner. Including feedback, each MN’s slow phase equation is

$$\dot{\psi}_j = G_{0j}(\psi_j - \psi_{\text{CPG}}) + \epsilon Z_j(\psi_j + \omega_0 t) [h_{s_j}^E(\psi_j + \omega_0 t, t) + h_{s_j}^I(\psi_j + \omega_0 t, t)], \tag{11}$$

(cf. Proctor et al. 2010), where the CPG phase $\psi_{\text{CPG}} = \omega_0 t$ for the left tripod ($j = 1 \dots 12$) and $\psi_{\text{CPG}} = \omega_0 t + \pi$ for the right tripod ($j = 13 \dots 24$), as noted in Sect. 2.3. Here $h_{s_j}^E$ and $h_{s_j}^I$ are excitatory and inhibitory proprioceptive inputs with reversal potentials $V_{\text{syn}}^{E/I}$, which take the forms $-s_{\pm,j}^{E/I}(t)[V_j(\psi_j + \omega_0 t) - V_{\text{syn}}^{E/I}]$, where $s_{\pm,j}^{E/I}$ are determined by Eq. (10). Such feedback generally depends explicitly

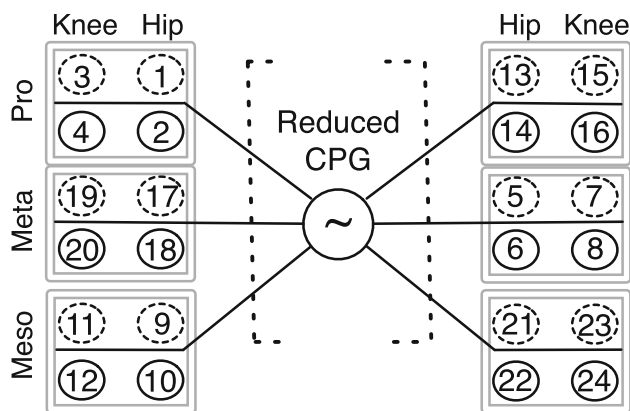


Fig. 3 The reduced CPG and motoneuron (MN) model. The CPG “clock” periodically modulates each leg’s hip and knee extensor (resp. flexor) MNs via inhibitory (resp. excitatory) synapses. Extensor and flexor MNs are denoted by dashed and solid circles, respectively; sensory inputs are not shown (cf. Fig. 2b)

on time t (because perturbations are unpredictable), but in unperturbed periodic running, it is $(2\pi/\omega_0)$ -periodic and phase-locked to the CPG, so these terms can further be averaged as in Sect. 2.3 to take the forms $H_{s_j}^{E/I}(\psi_j - \omega_0 t - \psi_{s_j}^{E/I})$, where $\psi_{s_j}^{E/I}$ specify the phases at which inputs arrive relative to ψ_{CPG} . See Proctor et al (2010, §2d) for more details. This paper and Ghigliazza and Holmes (2004a, §5) establish stability of the CPG-MN system, so we do not display eigenvalues for it here.

2.6 Summary of the full phase-reduced system

Before describing the performance of the phase-reduced model, we summarize its components and structure. The mechanical system’s state is given by the body center of mass position and velocity, body orientation and rotational velocity, and stance foot positions relative to the body. Muscle lengths $l_m(t)$ and velocities $v_m(t)$ can therefore be found from the body kinematics and leg geometry. The 6-oscillator CPG of Fig. 2a (left) is reduced to a clock running at the stepping frequency, emitting spikes that excite and inhibit the MNs at appropriate phase values. These in turn create muscle activations $a(t)$, thus determining muscle forces from Eq. (4) that are added to the passive stiffness and damping forces to form joint torques. (When proprioceptive feedback is included, MN spikes are added or deleted, and the activations accordingly modified.) Hence stance foot forces \mathbf{F}_j can be found and Eqs. (1)–(3) solved. The reduced system therefore has 24 oscillators for the MNs and 6 equations for the body mechanics: 30 first order ODEs in all.

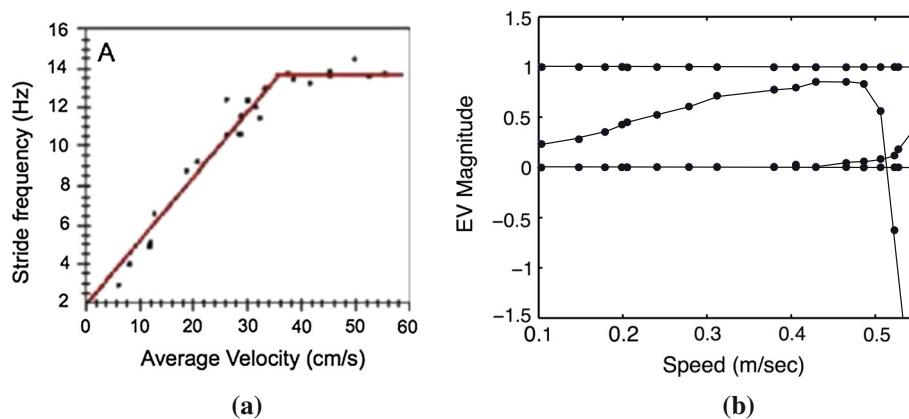


Fig. 4 **a** Stride frequency vs. speed for the cockroach *B. discoidalis* [solid dots, data from Ting et al. (1994), reproduced from Kukillaya and Holmes (2009)]. Solid red line shows the protocol of Kukillaya and Holmes (2009, §6), also used here. **b** Eigenvalues over the speed range of the phase-reduced model. Two eigenvalues remain near zero, corre-

sponding to the fast subspace on which perturbations decay quickly. One eigenvalue is unity due to yaw rotation invariance, and the fourth passes through -1 near 0.5 m s^{-1} , where stability is lost in a period-doubling bifurcation (Guckenheimer and Holmes 2002)

3 Stability over the animal's speed range

Legged animals can accelerate by increasing step frequency, extending stride length, or both. *B. Discoidalis* employs the former strategy up to $\approx 0.35 \text{ m s}^{-1}$, and lengthens strides above it (Ting et al. 1994). Under this protocol, the spring-actuated (Seipel et al. 2004; Kukillaya and Holmes 2007) and muscle-actuated (Kukillaya and Holmes 2009) models are stable up to 0.6 m s^{-1} , but stability can be lost if one departs too far from it (Seipel et al. 2004). In previous studies, the full neuromechanical model (Kukillaya et al. 2009) and its phase reduction (Proctor et al. 2010) were parameterized to produce a fixed running speed of 0.24 m s^{-1} , the CPG (stepping) frequency ω_0 being set at 9.93 Hz. We now show that the phase-reduced model, without feedback, also predicts stable running over much of the animal's speed range.

Following the lead of *B. Discoidalis*, we adopted the piecewise-linear frequency and stride-length protocol detailed in Kukillaya and Holmes (2009, §6), indicated by the solid (red) line on Fig. 4a. Step frequency was increased up to 0.375 m s^{-1} and strides were lengthened above 0.25 m s^{-1} by adjusting joint angles, and hence TD foot positions [also see Kukillaya and Holmes (2009, Supplementary Materials)]. Figure 4b shows the eigenvalues of the resulting stride-to-stride Poincaré map, indicating stability over the range $0.03\text{--}0.5 \text{ m s}^{-1}$. However, increasing ω_0 alone did not suffice to produce stable gaits over this entire range. As in Kukillaya and Holmes (2009) the scaling factor F_0 in Eq. (4) and the number of spikes in some MN bursts also had to be increased. Specific values were obtained via the inverse method described in that paper, and their trends were generally consistent with experimental observations on *B. discoidalis*. Without these adjustments, stability was lost at

$\approx 0.35 \text{ m s}^{-1}$. We comment on potential implications for legged robots in the first paragraph of the Discussion.

Unlike the models of Seipel et al. (2004) and Kukillaya and Holmes (2007, 2009), in which stability is lost at low or high speeds in pitchfork bifurcations to running in circles, here a period-doubling bifurcation occurs as a real eigenvalue passes through -1 at $\approx 0.5 \text{ m s}^{-1}$, producing orbits of period two (Guckenheimer and Holmes 2002). As we shall see in Sect. 4.1, these “limping” gaits can be stable, and they also lead to circular CoM trajectories.

4 Reflexive feedback, stability, and maneuverability

In this section, we extend our preliminary studies of the effects of inhibitory and excitatory feedback on recovery from impulsive perturbations (Proctor et al. 2010). We also investigate turning initiated by transient changes in TD positions and MN spike phases, and describe a trade-off between turning performance and stability in straight running.

4.1 Response to impulsive perturbations

As in previous studies (Kukillaya and Holmes 2007; Kukillaya et al. 2009), we applied impulsive lateral perturbations at the beginning of a left (L) stride, using the idealized triangular impulse described in those papers that approximates the miniature cannon used in the experiments of Jindrich and Full (2002). We allowed both excitatory and inhibitory conductances ($g_{\text{exc}}, g_{\text{inh}}$) to range over $[0, 0.4] \text{ mS cm}^{-2}$. For each pair of values, the phase-reduced model was integrated until it converged on a stable straight running gait at $\approx 0.24 \text{ m s}^{-1}$,

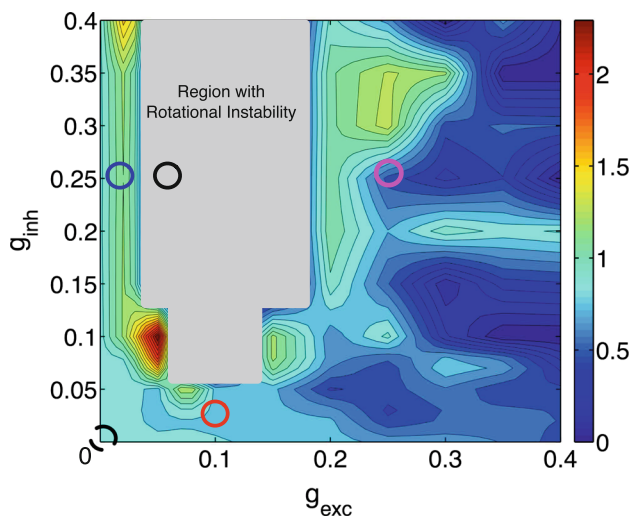


Fig. 5 Contour map showing overall heading changes in radians after impulsive lateral perturbation of the phase-reduced model, over the space (g_{exc} , g_{inh}) of excitatory and inhibitory sensory feedback conductances between sensory neurons and MNs. Circles identify parameter pairs that produce CoM trajectories shown in corresponding colors in Fig. 6. Gray band indicates region in which straight running is unstable

the impulse was applied, and the resulting heading change recorded after recovery to straight running. Figure 5 shows the overall heading changes, which can exceed 2 radians (115°). Straight running becomes unstable in the gray band of values around $g_{exc} = 0.1 \text{ mS cm}^{-2}$, for which we do not show heading changes. In this region, the stable gaits are L–R asymmetric and the model runs in circles, as described below.

To illustrate these results, in Fig. 6 (lower left) we show five CoM trajectories corresponding to different conductance pairs, including the no-feedback case ($(0, 0)$, dashed). One feedback case (blue, relatively high inhibition) turns more than the no-feedback case; two others (red, relatively high excitation; magenta, equally high excitation and inhibition) turn less. The CoM speed values at successive R and L TDs shown in Fig. 6 (right panels) also indicate more rapid convergence to the straight gait across these three cases. The fourth case (black) lies in the unstable region of Fig. 5, and its L (or R) TD speed switches between two values, while the R (or L) TD speed remains constant, so that the gait has period 2 with respect to a full L–R stride. Reflexive feedback has destabilized the straight gait in favor of circular paths, presumably via a period-doubling bifurcation analogous to that occurring at $\approx 0.5 \text{ m s}^{-1}$ without feedback, indicated in Fig. 4b).

Here we have kept all inhibitory and excitatory conductance pairs equal and have only applied feedback from sensors at knee joints. Among these examples, the equal conductance pair (magenta) gives the best perturbation rejection, but the right hand part of Fig. 5 indicates that even better rejection can be obtained for higher g_{exc} , although the results are sensitive to g_{inh} . Indeed, even finer tuning is

possible. Since 2 MNs activate each of the 6 joints in each tripod, and the 2 sensory neurons associated with each joint project to both MNs, the 24 synaptic conductances could be independently tuned to better match the magnitudes of the respective coupling functions, frequency differences, and distances from losing phase-locked behavior (cf. Eq. (11) and Fig. 7b).

4.2 Strategies for turning

Turns require changes in the body’s linear and angular momenta, the latter being increased and then decreased to resume straight running. This was achieved for the bipedal model in Proctor and Holmes (2008) by moving its hip joint forward and increasing the passive spring stiffness in the outer leg. The strategy was based on experiments in *B. discoidalis* indicating that momentum changes are likely generated by extending the outside front leg at TD (Jindrich and Full 1999) (its anterior extremum position r_{aep} increases $\approx 11\%$ over normal), and greater force production in the outside middle leg. These are illustrated by options 1 and 2 in Fig. 7a, exercised on the R and L tripods, respectively, in leftward turns. In contrast, in Sponberg et al. (2011), also using *B. Discoidalis*, it was found that advancing and augmenting MN spikes to the femoral extensor of the *inside* middle leg can produce a lateral impulse toward the leg, and a turn about a point beyond its foot: option 3 in Fig. 7a.

The present model, with its multi-jointed hexapedal geometry and musculature, is better equipped to test these strategies than the passive biped. TD positions can vary independently for each leg, and leg forces can be modulated by advancing or retarding MN bursts. In particular, firing an extensor MN early, while the muscle is still lengthening, generates large forces due to the velocity dependence in Eq. (4); cf. Proctor and Holmes (2010, Fig. 9). This is accomplished by changing MN frequency to $\omega_j + \epsilon(\delta_j + \delta_T)$, which modifies the averaged slow phase equation (8) to:

$$\dot{\psi}_j = \epsilon\delta_T + G_{0j}(\psi_j - \psi_{CPG}). \tag{12}$$

The resulting vertical shift in the RHS of Eq. (12) moves the fixed point; Fig. 7b shows the effect for the right middle hip extensor (MN $j = 5$ in Fig. 3).

We study turning in the absence of feedback, and as in Proctor and Holmes (2008) and Kukillaya et al. (2009) execute turns over three full strides. To turn left, we transiently increase the values of r_{aep} for the front right and/or δ_T for the middle right legs, respectively; all other parameters, including r_{aep} and δ_T for left legs, remain unchanged. At the end of the maneuver r_{aep} and δ_T return to their original values, allowing the model’s inherent stability to reduce counter-clockwise angular momentum and restore straight running. Fig. 8a shows the resulting heading changes over (r_{aep}, δ_T) -

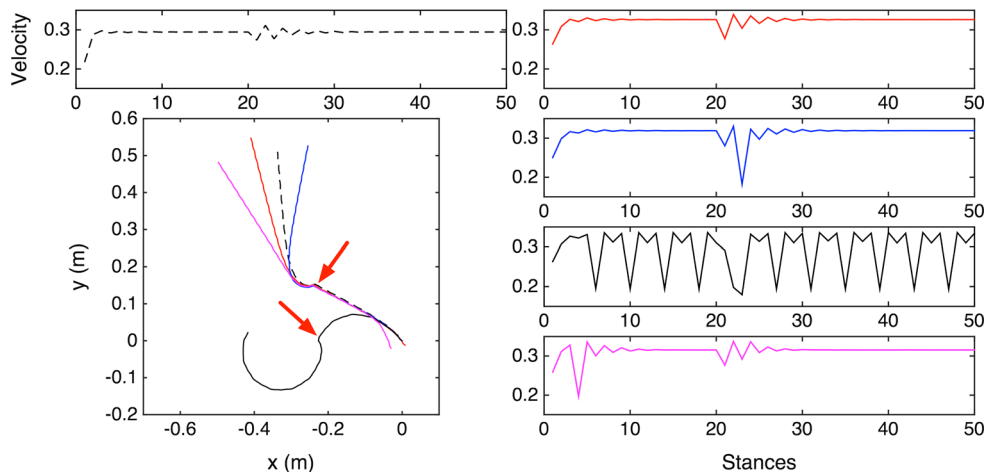


Fig. 6 Effects of torque feedback. Upper left panel shows CoM speed V at successive L and R TDs without feedback; lower left panel shows CoM trajectories for that case (dashed) and for 4 excitation/inhibition pairs $(g_{exc}, g_{inh}) = (0.025, 0.25)$ (blue), $(0.1, 0.025)$ (red), $(0.25, 0.25)$ (magenta) and $(0.075, 0.25)$ (black). In the latter case

straight running is unstable and the unperturbed body runs in circles. Red arrows indicate where lateral impulses were applied, at left TD of 20th stride. Right panels show CoM speeds at TD for the 4 cases with feedback, identified by color as in lower left panel and in Fig. 5

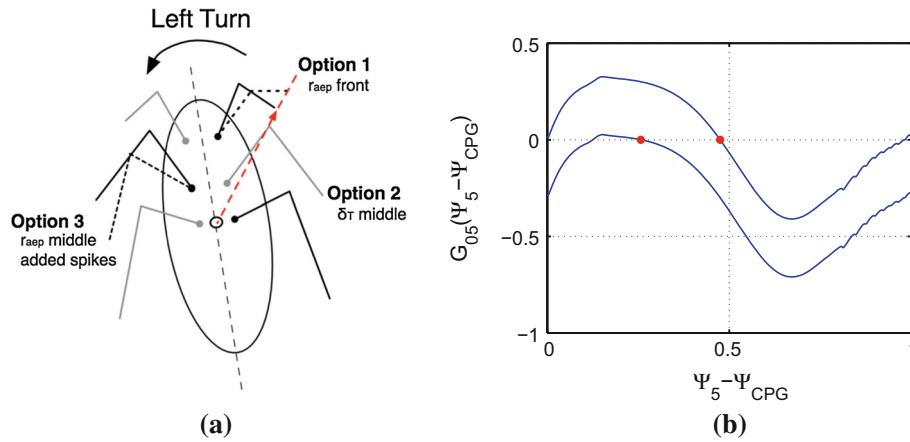
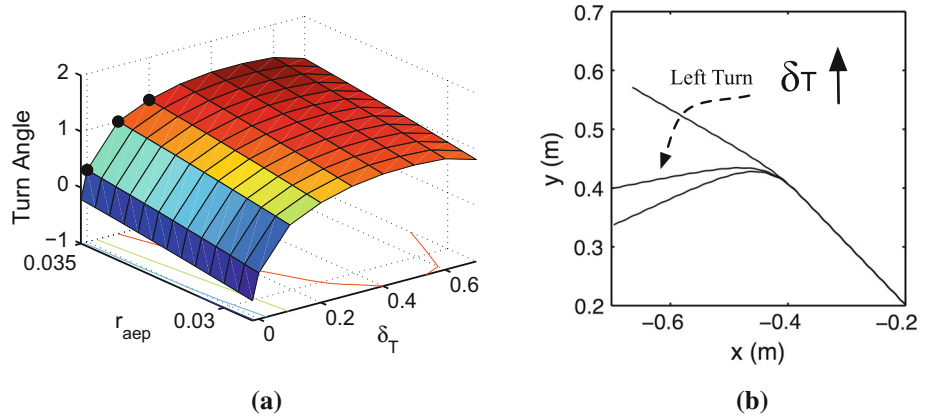


Fig. 7 **a** Three strategies for executing a left turn: (1) extend the right front left leg radially at TD; (2) change the timing of the extensor MN burst of the right middle leg, and/or (3) change the duty cycle of the left middle leg by adding MN spikes. **b** The effect of adding $\delta_T > 0$

(upper curve) to the averaged coupling function $G_{05}(\psi_5 - \psi_{CPG})$ (lower curve): the fixed point (filled circle), defining phase difference between MN and CPG, shifts rightwards, advancing extensor activation

Fig. 8 **a** Net turning angles (radians) of the feedforward phase-reduced model for 3-stride turns, over the (r_{aep}, δ_T) parameter plane. **b** Three CoM trajectories for parameters $(r_{aep}, \delta_T) = (0.035, 0)$, $(0.035, 0.1)$, and $(0.035, 0.2)$, points indicated by filled circles in **a**



parameter space, and Fig. 8b shows three examples of CoM trajectories that undergo larger turns as δ_T moves from 0 to 0.2. We allowed r_{aep} to increase by up to 17% over its normal value 0.03 m from CoM, and δ_T to change fixed point positions by up to ≈ 1.9 radians (cf. Fig. 7b).

We found that turns of up to $\approx 12^\circ$ can be executed by changing r_{aep} alone, and that adjustment of δ_T , especially near $\delta_T = 0$, substantially amplifies these, yielding turns of up to 85° . The sensitivity near $\delta_T = 0$ can be explained by examining Fig. 7b: small variations in δ_T cause large changes in fixed point phase, because the slope of the coupling function is small at the stable fixed point for $\delta_T = 0$; moreover, the slope at the “new” fixed point is larger, implying fast attraction to it, further increasing the turn angle. [Negative shifts in δ_T would destroy both fixed points in a saddle-node bifurcation (Guckenheimer and Holmes 2002).]

A different strategy was used in Kukillaya et al. (2009): muscle activations were unchanged, TD positions alone were modified. To turn left, the right (outside) front and hind feet were placed further forward and the left (inside) middle foot further backward at R TD, producing an additional positive counterclockwise moment about the CoM throughout the stance period. This mimics the effect of earlier activation of the extensor for the inside middle leg, as in Sponberg et al. (2011, Fig. 7), since that opposes the flexor and cuts short the swing phase, moving TD backwards. The phase-reduced model can achieve the same effect by moving the fixed point as in Fig. 7b, but for the *inside* hip extensor MN. We do not explore this option here.

The turning experiments of Jindrich and Full (1999) predict that the outside middle leg produces much of the force that changes linear momentum, while the extended TD position of the outside front leg generates the angular change. Our current results show that increased force production at the outside middle leg has a larger effect than front foot placement, in contrast with the bipedal study (Proctor and Holmes 2008), which found that hip placement had a more significant effect than stiffening the passive leg. The difference between the energy-conserving biped and the present actuated model may be due to latter’s ability to do significant positive and negative work during a stance phase (Kukillaya and Holmes 2009, Fig. 10) and to produce larger turning moments with its three stance legs.

In all cases studied, relatively small changes in biophysically relevant parameters can produce large turns in these models, by breaking the L–R symmetry and creating a transient rotational instability. This is clearly advantageous for an insect that needs to be highly maneuverable, and it offers engineers insight into implementing turns in legged robots; see Hoover et al. (2010) for an example.

5 More perturbations, climbing, and exteroceptive feedback

We now use the phase-reduced model to simulate experiments in which a cockroach runs on a moving platform, carrying a backpack that changes its mass and moment of inertia. We then investigate climbing by introducing a gravitational component that breaks rotational symmetry. Finally, we superimpose on the turning mechanism of Sect. 4.2 a simple linear controller for goal-oriented steering. To better identify the effects of these treatments, throughout this section we exclude proprioceptive feedback.

5.1 Perturbations due to a moving platform and backpack

As noted in Sect. 4.1, the perturbation experiments of Jindrich and Full (2002) used a miniature cannon mounted on the insect’s back. Model simulations of this appeared in Kukillaya et al. (2009) and Proctor et al. (2010). A more recent experiment imparts a lateral impulse by accelerating a platform on which the insect runs (Mongeau et al. 2012; Revzen et al. 2013), allowing a wider range of better-controlled conditions. The insect’s mass and moment of inertia can be increased by adding elements to a backpack carrying microaccelerometers (Moore et al. 2010).

In the platform experiments, a range of accelerations were investigated, from 0.6 ± 0.1 to 1.5 ± 0.2 g over 100 ms intervals (Moore et al. 2010; Revzen et al. 2013). We based our simulations on earlier work, in which shorter acceleration periods were used (S. Burden, personal communication). Our platform accelerates from 0 to 0.05 ms^{-1} over ≈ 40 ms, imparting 1.25 g. We simulate the substrate movement by displacing the model’s feet laterally, at constant acceleration, during a single stance phase, implicitly assuming that no sliding occurs.

Figure 9 illustrates recovery of the phase-reduced model for both the platform and cannon perturbations. The effects of the former on CoM speed and body orientation are much weaker than those of the cannon, but recovery from perturbations is monotonic in both cases: all state variables decay from stance to stance in a manner consistent with real, stable eigenvalues in the linearized Poincaré map. Here the residual body orientation $\theta_{\text{pert}}(t) - \theta_{\text{unpert}}(t)$, the difference between orientations for perturbed and unperturbed runs, is plotted. The decrease in forward CoM velocity in the platform simulation is similar to that of Revzen et al. (2013, Fig. 4C), but the lateral velocity response is much weaker (not shown here). This may be caused by our shorter acceleration duration or is possibly due to the insect’s feet sliding during the perturbation.

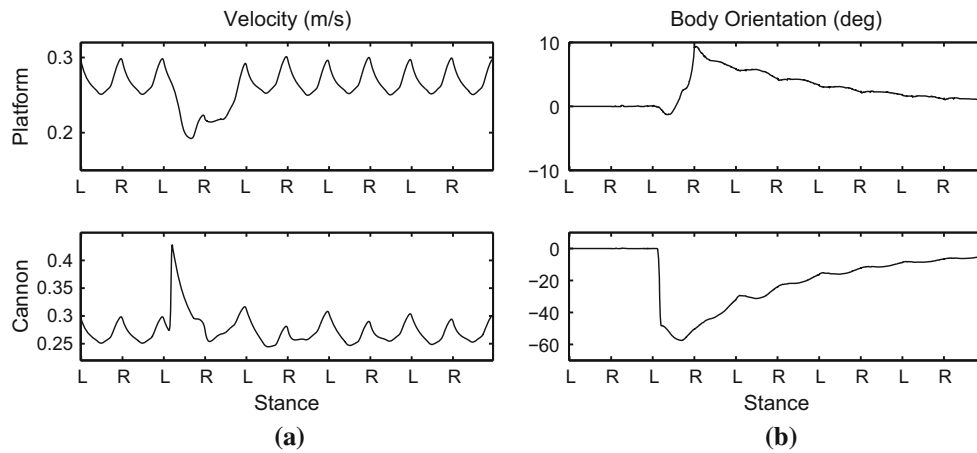


Fig. 9 CoM speeds v and residual body orientations $\theta_{\text{pert}} - \theta_{\text{unpert}}$ during perturbations by the moving platform (top) and rapid impulse device (bottom). R/L denote liftoff and touchdown events; perturbations begin in second L stance and last ≈ 40 ms for platform and 4 ms for cannon

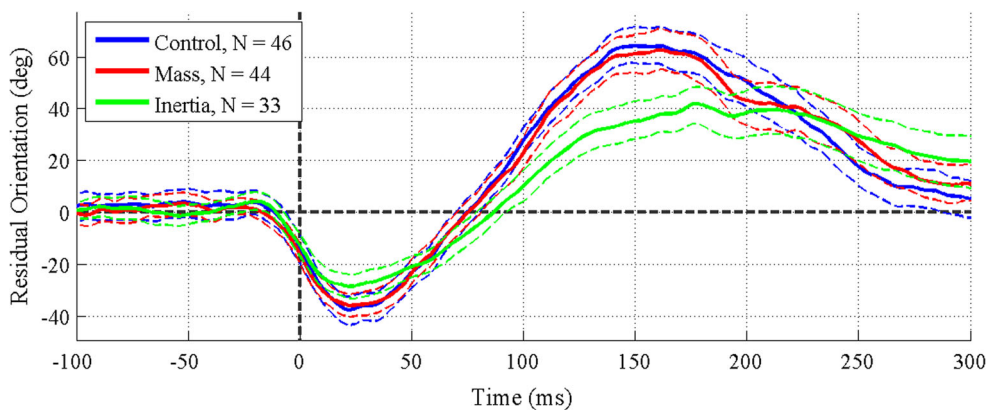


Fig. 10 Residual body orientations $\theta_{\text{pert}} - \theta_{\text{unpert}}$, averaged over multiple (N) experimental runs. Three conditions are shown: control with “bare” backpack (blue); 90% increase in mass (red), and 960% increase

in moment of inertia (green). Solid lines show means; dashed lines indicate standard errors. . Figure courtesy of S. Revzen, S. Burden, T. Moore, J-M. Mongeau, and R. Full

Figure 10 shows residual body orientations for a control condition experiment with the backpack alone, and for experiments with increased mass and substantially increased moment of inertia. Note that residual body orientation changes sign over the course of 300 ms (≈ 4 –8 steps, cf. Fig. 10), implying that the velocity vector relative to body centerline should change likewise (Revzen et al. 2013). This is incompatible with the model’s real eigenvalues, an observation to which we return in Sect. 5.3.

Figure 11(top) repeats the results of Fig. 9(right) and also shows residual orientations for the model with increased mass and moment of inertia, and Fig. 12 illustrates how these treatments affect the eigenvalues. Typical mass and moment of inertia of *B. discoidalis* are shown, along with the largest experimental values tested (Revzen et al. 2013), and values at which the model becomes unstable. Stability is lost at $\approx 50\%$ mass increase, substantially below the 90% value tested (Fig. 12a: hence we show a response for 40%

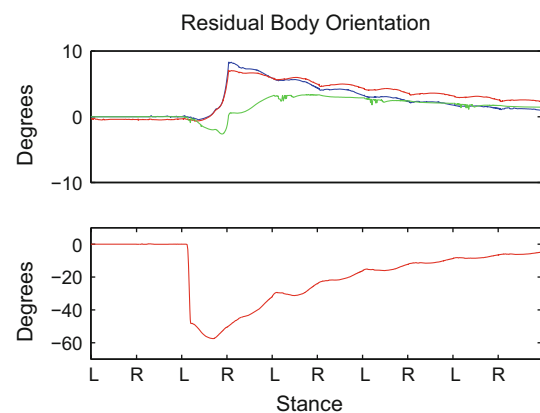


Fig. 11 Residual body orientations $\theta_{\text{pert}} - \theta_{\text{unpert}}$ for model simulations of platform (top) and cannon (bottom) experiments. Colors at top correspond to the cases of Fig. 10: control (blue); 40% mass increase (red), and 960% moment of inertia increase (green)

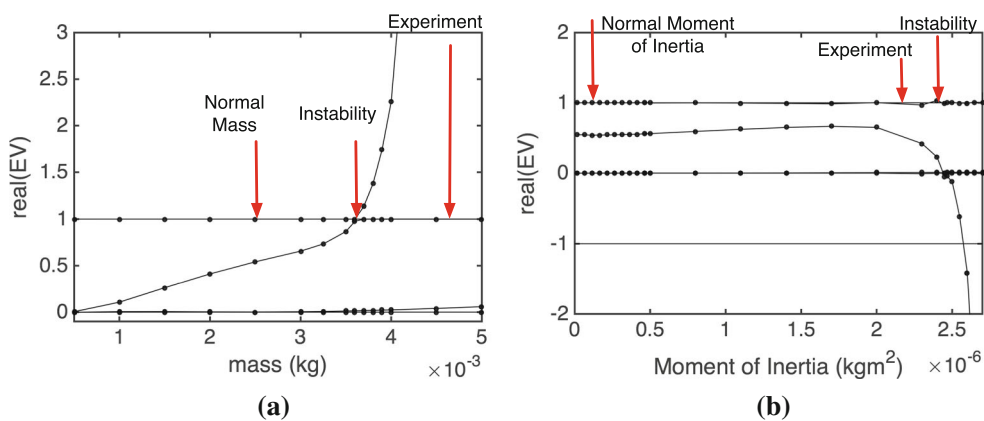


Fig. 12 Eigenvalues of the phase-reduced model linearized at the straight gait at preferred running speed 0.24 ms^{-1} as mass **(a)** and moment of inertia **(b)** are varied. Arrows indicate typical parameter

values for normal insect, values at which straight running becomes unstable, and the largest values used in experiments of Revzen et al. (2013), cf. Fig. 10

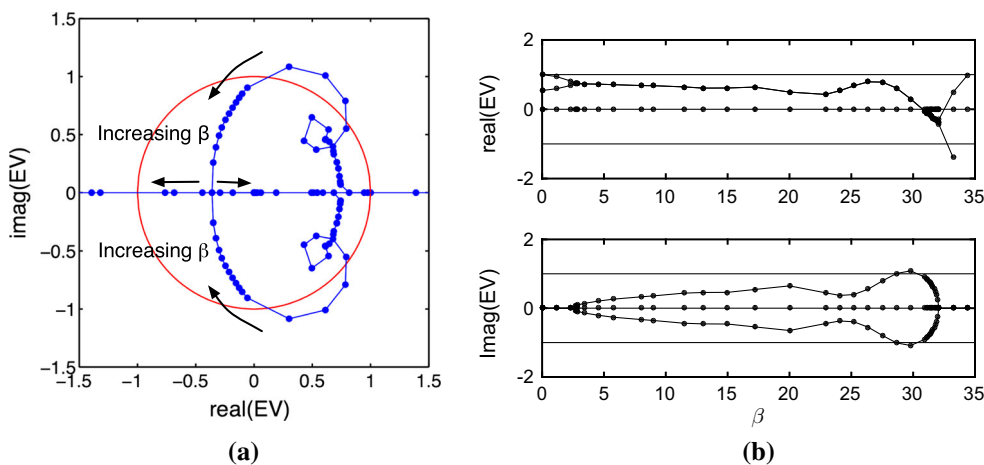


Fig. 13 Eigenvalue paths for the feedforward phase-reduced model with increasing external force as described in the text, representing running up ramps of increasing angle β . **a** Paths in the complex plane; **b** real and imaginary parts

increase in Fig. 11). Despite this, recovery is qualitatively similar to the observations of Fig. 10: residual orientations of the normal and increased mass cases are close, and the decay rate of the latter is slightly slower. In contrast, the stability boundary for increased moment of inertia is somewhat higher than the experimentally tested values, predicting that the insect can sustain more than twelvefold increases while remaining stable. Also, the magnitude of the slow eigenvalue modestly increases up to $\approx 900\%$ increase in moment of inertia (Fig. 12b), indicating a slower recovery rate, in qualitative agreement with the green trajectory of Fig. 10.

5.2 Climbing

Cockroaches employ double-tripod gaits for level running and climbing, but foot force directions can differ radically between these behaviors. Forces typically point outward in horizontal running, but inward (toward the CoM) and down-

ward in vertical climbing, allowing the insect to advance against gravity (Goldman et al. 2006). To understand the transition from level running to climbing, cockroaches have been run up ramps of increasing angle (Jayaram et al. 2010), and a simple model has been developed based on the bipedal point mass model of Schmitt and Holmes (2000). This uses passively sprung legs and can produce stable gaits over a substantial range of speeds on both uphill and downhill slopes (Schmitt and Bonnono 2009).

Here we investigate the stability of climbing by applying a constant force $F_{\text{grav}} = -mg \sin \beta \hat{i}$ at the CoM, opposing the running direction $+\hat{i}$ in the inertial frame. Here g is gravitational acceleration and β the ramp angle. All other parameters are unchanged. Figure 13 shows eigenvalues of the Poincaré map linearized about straight running. As β increases from zero and rotational invariance is lost, the unit eigenvalue (cf. Fig. 4b) drops below 1 and collides with the weak eigenvalue

to produce a complex-conjugate pair that briefly leave and reenter the unit circle, subsequently meeting on the real axis before an eigenvalue passes through -1 in a period-doubling bifurcation at $\beta \approx 33^\circ$. When all four eigenvalues lie inside the unit circle, the climbing gait is (fully) asymptotically stable.

Insects can ascend vertical walls (Goldman et al. 2006), while our model loses stability on a modest incline. However, we have not modified muscle activations $a(t)$, scale factors F_0 [cf. Eq. (4)] or other parameters chosen for level running. Indeed, lacking individual foot force and position data on sloping substrates, we cannot carry out the inverse fitting procedure of Kukillaya and Holmes (2009) to match lateral leg forces that push outward for $\beta = 0$ and transition to pulling in as the slope steepens. Such parameter tuning, with or without proprioceptive feedback, could stabilize climbing over a wider range.

Here gravity breaks the rotational symmetry and introduces a preferred direction, stabilizing the neutral rotational mode and eliminating all other solutions except downhill running in the direction $-\hat{\mathbf{i}}$, which we find to be unstable for all but very small negative angles β (simulation results not shown). Rotational symmetry is also broken by the insect’s preferences to seek dark areas and avoid touching the platform’s side walls, qualities used in experiments to encourage straight running. These facts, and particularly the generation of complex-conjugate eigenvalues, partially motivate our final study of a simple control algorithm for steering.

5.3 Steering by exteroceptive feedback

Previous work investigated how feedback from antennae can guide cockroaches in running along walls (Cowan et al. 2006), leading to a control algorithm built on the passive bipedal model that maintains distance from the wall (Lee et al. 2008). Little is known about other navigation mechanisms, so here we take a more abstract viewpoint, assuming merely that exteroceptive sensing provides a desired direction in inertial space that the animal seeks to follow. We show that a simple state feedback system can accomplish this, and that the resulting dynamics has stability characteristics consistent with the insect’s behavior in the platform perturbation experiment of Mongeau et al. (2012) and Revzen et al. (2013) (Sect. 5.1).

We adopt the two strategies of Sect. 4.2 (options 1 and 2, Fig. 7), using extension of the outside front leg and relative phase of the hip extensor MN of the outside middle leg as feedback control inputs. These are applied at TD and held throughout each stance phase, as in feedforward turning. We may still use a Poincaré map, but it must be composed of separate maps for L and R stance phases, since different feedback will generally be applied at every TD. These maps are defined as

$$(v_{n+1}, \delta_{n+1}, \theta_{n+1}, \omega_{n+1}) = P^L (v_n, \delta_n, \theta_n, \omega_n, \mathbf{u}_n), \quad (13)$$

$$(v_{n+2}, \delta_{n+2}, \theta_{n+2}, \omega_{n+2}) = P^R (v_{n+1}, \delta_{n+1}, \theta_{n+1}, \omega_{n+1}, \mathbf{u}_{n+1}), \quad (14)$$

where $\mathbf{u} = (\delta_T^L, \delta_T^R, r_{\text{aep}}^L, r_{\text{aep}}^R)$ is the control input and $P = P^R \cdot P^L$. We compute linearized maps DP^R and DP^L at a fixed point $\mathbf{x}_n = \mathbf{x}^{*L/R} + \bar{\mathbf{x}}_n$, where $\bar{\mathbf{x}}_n = (v_n, \delta_n, \theta_n, \omega_n)$ represents deviation from an uncontrolled straight gait with L and R TD states \mathbf{x}^{*L} , \mathbf{x}^{*R} and preferred running direction θ^* , and $\mathbf{u}_n = \mathbf{u}^* + \bar{\mathbf{u}}_n$ is the control input. This yields a discrete linear control system:

$$\bar{\mathbf{x}}_{n+1} = \mathbf{A}^L \bar{\mathbf{x}}_n + \mathbf{B}^L \bar{\mathbf{u}}_n, \quad (15)$$

$$\bar{\mathbf{x}}_{n+2} = \mathbf{A}^R \bar{\mathbf{x}}_{n+1} + \mathbf{B}^R \bar{\mathbf{u}}_{n+1}, \quad (16)$$

in which the matrices \mathbf{A}^L , \mathbf{A}^R are the linearized L and R stance maps without control, and \mathbf{B}^L , \mathbf{B}^R express the effects of the control inputs $(\delta_T^L, r_{\text{aep}}^L)$ and $(\delta_T^R, r_{\text{aep}}^R)$ on the left and right tripods. Hence the second and fourth columns of \mathbf{B}^L , and the first and third of \mathbf{B}^R , are zeroes.

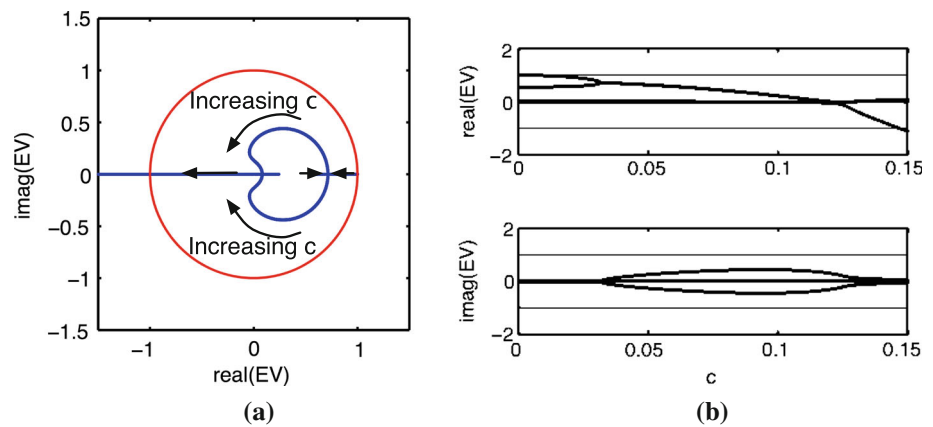
We implement a state feedback strategy $\bar{\mathbf{u}}_j = \mathbf{K}\bar{\mathbf{x}}_j$ that provides a control input $\bar{\mathbf{u}}_j$ at the j ’th TD based on current deviation θ_j from θ^* . The same matrix \mathbf{K} is used in both L and R stance maps because the matrices \mathbf{B}^L , \mathbf{B}^R direct feedback to the appropriate legs. For simplicity, we choose all entries in \mathbf{K} to be zero except the third column $c\mathbf{1}$ that weights deviations θ_j with uniform gain c over the four state variables. Equations (15) and (16) can now be combined into a full L-L linearized stride map describing the local dynamics of the controlled system:

$$\bar{\mathbf{x}}_{n+2} = (\mathbf{A}^R + \mathbf{B}^R \mathbf{K})(\mathbf{A}^L + \mathbf{B}^L \mathbf{K}) \bar{\mathbf{x}}_n \stackrel{\text{def}}{=} \mathbf{G} \bar{\mathbf{x}}_n. \quad (17)$$

Figure 14 shows how the two largest eigenvalues of \mathbf{G} change as gain increases, colliding and becoming complex conjugates until they again become real and one of them passes through -1 . Here, unlike Fig. 13, all eigenvalues remain inside the unit circle until the period-doubling bifurcation, implying that the controlled system is stable. This model also shows that a single state feedback system regulating steering can produce complex eigenvalues, as observed in climbing and implicit in the insect’s damped yaw oscillation during recovery from the platform perturbation: Fig. 10. In all these cases, a preferred direction breaks rotational symmetry, allowing the neutral eigenvalue to enter the unit circle and hence produce oscillatory dynamics. In this regard, exteroceptive feedback could produce the response observed in the platform perturbation experiment.

Finally, we note that one could use different weights in \mathbf{K} , and/or add feedback from angular velocity ω_n , to better match the data or potentially improve performance.

Fig. 14 Eigenvalue paths for the phase-reduced model with heading feedback Eq. (17), but without proprioception, as gain c increases. The strongly stable eigenvalue pair remain of size $\mathcal{O}(10^{-2})$ and a period-doubling bifurcation occurs at $c \approx 0.15$. See text for further details



6 Conclusion and discussion

This paper extends our earlier study of the dynamics and stability of a phase-reduced, hexapedal, neuromechanical model for insect locomotion (Proctor et al. 2010) (Figs. 1, 2, 3). By increasing both stepping frequency and stride length and adjusting motoneuron outputs and muscle forces in agreement with earlier work (Seipel et al. 2004; Kukillaya and Holmes 2007, 2009), we found stable gaits over most of the cockroach’s typical speed range (Fig. 4). These parameter variations with speed are consistent with cockroach behavior, in which frequency initially increases and stride lengths increase at higher speeds, allowing the animal to remain within a stable region in parameter space. Specifically, the mechanical models in Seipel (2004, Fig. 14) and Kukillaya and Holmes (2007, Figs. 11, 12) display unstable regions outside a diagonal channel in speed-stride frequency space. Since neither model contains neural components or proprioceptive feedback, the observation on stepping frequency and stride length may be useful in designing legged robots that operate over wide speed ranges.

We then showed that reflexive feedback of joint torques to motoneurons can modulate the response to impulsive lateral perturbations. Specifically, an appropriate balance of excitation and inhibition can reduce heading changes (Figs. 5, 6). Moreover, straight running gaits can be destabilized by changing foot positions and muscle forces, moving the center of pressure and creating transient growth in body angular velocity to make turns. Small changes in front leg touchdown positions and timing of middle-leg extensor activations can produce turns of almost 90° within three strides (Figs. 7, 8). Thus, the model can be steered by small modulations, as in Proctor and Holmes (2008) and Kukillaya and Holmes (2009), confirming the findings of Jindrich and Full (1999) that changes in the symmetric double-tripod gait can lead to substantial turns and revealing a mechanism that achieves this. [See the section “Turning dynamics can be characterized as a minor modification of straight-ahead running” in Jindrich

and Full (1999).] However, depending on the balance of excitation and inhibition, reflexive feedback can negatively affect turning performance.

To further investigate this, we computed eigenvalues of the Poincaré map for the four stable cases of Fig. 6 (blue, red, magenta and dashed). The unit eigenvalue and strongly stable pair remained essentially unchanged, but the weakly stable eigenvalue increased to 0.60 and 0.58 for the blue and red trajectories, and decreased to 0.47 for magenta, compared to 0.54 without feedback, partly consistent with better rejection of the perturbation. These four cases also illuminate how feedback can affect turning. Setting $r_{aep} = 0.035$ and $\delta_T = 0.2$, which yields a 1.24 radian turn without feedback (Fig. 8, Sect. 4.2), the blue, red and magenta cases, respectively, produce turns of 0.93, 0.69 and 0.72 radians, all smaller than the feedforward case, illustrating a trade-off between maneuverability and stability.

A study of the knifefish *Eigenmannia virescens* that also uses a robot and mathematical models (Sefati et al. 2013) shows that such a trade-off can be eliminated by producing mutually opposing forces. Defining stability as “the resistance to and recovery from disturbances to an intended trajectory,” and maneuverability as “the relative amplitude of the control signal required to change movement direction,” the authors argue that forces generated by counter-propagating waves in the fish’s ribbon fin can simultaneously stabilize station-keeping and enhance maneuverability. Here we also characterize stability via eigenvalues of the Poincaré map Eq. (5), as in Full et al. (2002), and gauge maneuverability by the magnitude of turns (cf. Fig. 8). We find that two of our Poincaré map’s four eigenvalues typically remain small, conferring passive stability in those modes, while the other two are closer to 1, indicating potential instability. An earlier study (Proctor and Holmes 2008) showed that allowing an eigenvalue to cross the unit circle for a few strides destabilizes forward running, resulting in sharp turns due to the intrinsic nonlinear dynamics prescribed by the body-leg mechanics of locomotion in the ground plane.

In the present work, two parameters can control turning, as realized via outer front leg TD placement and timing of MN spikes to the outer middle-leg hip extensor in Sect. 5.3 (also see Sect. 4.2 and Figs. 7–8). We believe that this mechanism is analogous to moving the node between the ribbon waves and tuning their frequency in Sefati et al. (2013). That study also suggests that two control parameters can modulate a fairly complex behavior. The fact that two modes—a neutral and a weakly stable or unstable eigenvalue—are important in cockroach turning, as noted again below, suggests that the insect's dynamics offer a similar trade-off between maneuverability and stability. Future studies should estimate the work required for steering to allow quantitative comparisons, as in Sefati et al. (2013, and Supplementary Information for that paper).

We also examined responses to uniform acceleration of the ground plane, to increases in mass and moment of inertia (Figs. 9, 10, 11, 12), and changes in stability caused by ascending a slope (Fig. 13). Finally, we developed a simple feedback controller that actuates the steering mechanism to maintain a desired heading (Fig. 14).

Throughout, we find that a weakly stable eigenvalue plays a key role in the model's response to perturbations, as described above and previously in Kukillaya and Holmes (2009, §7). When climbing against a gravitational field (Sect. 5.2) or subject to control that maintains heading direction (Sect. 5.3), this eigenvalue interacts with an otherwise neutral, unit eigenvalue associated with yaw, generating an oscillatory mode which can become unstable. Understanding how actuation and feedback influence these critical modes would further illuminate control systems employed by insects and suggest mechanisms for controlling legged robots. In summary, our work shows that a relatively simple phase-reduced model allows inclusion of neural feedback while capturing key aspects of dynamical behavior, so we believe it could contribute significantly to such studies.

Acknowledgements This work was partially supported by NSF EF-0425878 (Frontiers in Biological Research), NSF DMS-1430077 (CRCNS U.S.-German Collaboration) and Princeton's J. Insley Blair Pyne Fund. We thank the anonymous reviewers for their useful suggestions and for helping us to correct several errors.

References

- Ahn A, Full R (2002) A motor and a brake: two leg extensor muscles acting at the same joint manage energy differently in a running insect. *J Exp Biol* 205:379–389
- Ahn A, Meijer K, Full R (2006) In situ muscle power differs without varying in vitro mechanical properties in two insect leg muscles innervated by the same motor neuron. *J Exp Biol* 209:3370–3382
- Altendorfer R, Moore N, Komsuoglu H, Buehler M, Brown HB Jr, McMordie D, Saranli U, Full R, Koditschek D (2001) RHex: a biologically inspired hexapod runner. *Auton Robots* 11:207–213
- Brown I, Scott S, Loeb G (1995) Preflexes—programmable high-gain zero-delay intrinsic responses of perturbed musculoskeletal systems. *Soc Neurosci Abstr* 21(562):9
- Couzin-Fuchs E, Kiemel T, Gal O, Holmes P, Ayali A (2015) Intersegmental coupling and recovery from perturbations in freely-running cockroaches. *J Exp Biol* 218:285–297
- Cowan N, Lee J, Full R (2006) Task-level control of rapid wall following in the american cockroach. *J Exp Biol* 209:1617–1629
- David I, Holmes P, Ayali A (2016) Endogenous rhythm and pattern generating circuit interactions in cockroach motor centers. *Biol Open* 5:1229–1240
- Delcomyn F (1980) Neural basis of rhythmic behaviors in animals. *Science* 210:492–498
- Delcomyn F (2004) Insect walking and robotics. *Annu Rev Entomol* 49:51–70
- Electronic Physics Auxiliary Publication Service E (2009) See document no. e-chaoh-19-005992 for parameter values and code documentation. <http://ftp.aip.org/epaps/chaos/E-CHAOEH-19-005992/>. For more information on EPAPS, see <http://www.aip.org/pubservs/epaps.html>
- Fuchs E, Holmes P, Kiemel T, Ayali A (2011) Intersegmental coordination of cockroach locomotion: adaptive control of centrally coupled pattern generator circuits. *Front Neural Circuits* 4:125
- Fuchs E, Holmes P, David I, Ayali A (2012) Proprioceptive feedback reinforces centrally-generated stepping patterns in the cockroach. *J Exp Biol* 215:1884–1891
- Full R, Koditschek D (1999) Templates and anchors: neuromechanical hypothesis of legged locomotion on land. *J Exp Biol* 202:3325–3332
- Full R, Tu M (1991) Mechanics of a rapid running insect: two-, four- and six-legged locomotion. *J Exp Biol* 156:215–231
- Full R, Kubow T, Schmitt J, Holmes P, Koditschek D (2002) Quantifying dynamic stability and maneuverability in legged locomotion. *Integr Comp Biol* 42:149–157
- Ghigliazza R, Holmes P (2004a) A minimal model of a central pattern generator and motoneurons for insect locomotion. *SIAM J Appl Dyn Syst* 3(4):671–700
- Ghigliazza R, Holmes P (2004b) Minimal models of bursting neurons: how multiple currents, conductances and timescales affect bifurcation diagrams. *SIAM J Appl Dyn Syst* 3(4):636–670
- Goldman D, Chen T, Dudek D, Full R (2006) Dynamics of rapid vertical climbing in a cockroach reveals a template. *J Exp Biol* 209:2990–3000
- Guckenheimer J, Holmes P (2002) *Nonlinear Oscillations, Dynamical Systems and Bifurcations of Vector Fields*, 6th edn. Springer, Berlin
- Guckenheimer J, Johnson S (1995) Planar hybrid systems. In: *Lecture notes in computer science* No. 999, Springer, Berlin, pp 202–225
- Hill A (1938) The heat of shortening and the dynamic constants of muscle. *Proc R Soc Lond B* 126:136–195
- Holmes P, Full R, Koditschek D, Guckenheimer J (2006) The dynamics of legged locomotion: models, analyses and challenges. *SIAM Rev* 48(2):207–304
- Hoover A, Burden S, Fu X, Sastry S, Fearing R (2010) Bio-inspired design and dynamic maneuverability of a actuated six-legged robot. In: *Proceedings of IEEE international conference on biomedical robotics and biomechatronics (BIOROB)*, pp 869–876
- Jayaram K, Mongeau JM, McRae B, Full R (2010) High-speed horizontal to vertical transitions in running cockroaches reveals a principle of robustness. In: *Society for Integrative and Comparative Biology*. <http://www.sicb.org/meetings/2010/schedule/abstractdetails.php?id=1109>
- Jindrich D, Full R (1999) Many-legged maneuverability: dynamics of turning in hexapods. *J Exp Biol* 202:1603–1623
- Jindrich D, Full R (2002) Dynamic stabilization of rapid hexapedal locomotion. *J Exp Biol* 205:2803–2823

- Kram R, Wong B, Full R (1997) Three-dimensional kinematics and limb kinetic energy of running cockroaches. *J Exp Biol* 200:1919–1929
- Kubow T, Full R (1999) The role of the mechanical system in control: a hypothesis of self stabilization in hexapedal runners. *Philos Trans R Soc Lond B* 354:849–861
- Kukillaya R, Holmes P (2007) A hexapedal jointed-leg model for insect locomotion in the horizontal plane. *Biol Cybern* 97:379–395
- Kukillaya R, Holmes P (2009) A model for insect locomotion in the horizontal plane: feedforward activation of fast muscles, stability, and robustness. *J Theor Biol* 261(2):210–226
- Kukillaya R, Proctor J, Holmes P (2009) Neuro-mechanical models for insect locomotion: stability, maneuverability, and proprioceptive feedback. *CHAOS Interdiscip J Nonlinear Sci* 19(2):026107
- Lee J, Sponberg S, Loh O, Lamperski A, Full R, Cowan N (2008) Templates and anchors for antenna-based wall following in cockroaches. *IEEE Trans Robot* 24(1):130–143
- Mongeau JM, Alexander T, Full R (2012) Neuromechanical feedback during dynamic recovery after a lateral perturbation in rapid running cockroaches. In: *Society for Integrative and Comparative Biology*. <http://www.sicb.org/meetings/2012/schedule/abstractdetails.php?id=555>
- Moore T, Revzen S, Burden S, Full R (2010) Adding inertia and mass to test stability predictions in rapid running insects. In: *Society for Integrative and Comparative Biology*. <http://www.sicb.org/meetings/2010/schedule/abstractdetails.php?id=1290>
- Pearson K (1972) Central programming and reflex control of walking in the cockroach. *J Exp Biol* 56:173–193
- Pearson K, Iles J (1970) Discharge patterns of coxal levator and depressor motoneurons in the cockroach *Periplaneta americana*. *J Exp Biol* 52:139–165
- Pearson K, Iles J (1971) Innervation of the coxal depressor muscles in the cockroach *Periplaneta americana*. *J Exp Biol* 54:215–232
- Pearson K, Iles J (1973) Nervous mechanisms underlying intersegmental co-ordination of leg movements during walking in the cockroach. *J Exp Biol* 58:725–744
- Proctor J, Holmes P (2008) Steering by transient destabilization in piecewise-holonomic models of legged locomotion. *Regul Chaotic Dyn* 13(4):267–282
- Proctor J, Holmes P (2010) Reflexes and preflexes: on the role of sensory feedback on rhythmic patterns in legged locomotion. *Biol Cybern* 2:513–531
- Proctor J, Kukillaya R, Holmes P (2010) A phase-reduced neuro-mechanical model for insect locomotion: feed-forward stability and proprioceptive feedback. *Philos Trans R Soc A* 368:5087–5104
- Revzen S, Burden S, Moore T, Mongeau JM, Full R (2013) Instantaneous kinematic phase reflects neuromechanical response to lateral perturbations of running cockroaches. *Biol Cybern* 107:179–200
- Schmitt J, Bonnono S (2009) Dynamics and stability of lateral plane locomotion on inclines. *J Theor Biol* 261:598–609
- Schmitt J, Holmes P (2000) Mechanical models for insect locomotion: dynamics and stability in the horizontal plane—I. *Theory Biol Cybern* 83(6):501–515
- Schmitt J, Holmes P (2003) Mechanical models for insect locomotion: active muscles and energy losses. *Biol Cybern* 89(1):43–55
- Schmitt J, Garcia M, Razo RC, Holmes P, Full RJ (2002) Dynamics and stability of legged locomotion in the horizontal plane: a test case using insects. *Biol Cybern* 86(5):343–353
- Sefati S, Neveln I, Roth E, Mitchell T, Snyder J, MacIver M, Fortune E, Cowan N (2013) Mutually opposing forces during locomotion can eliminate the tradeoff between maneuverability and stability. *Proc Natl Acad Sci* 110(47):18798–18803
- Seipel J, Holmes P, Full R (2004) Dynamics and stability of insect locomotion: a hexapedal model for horizontal plane motion. *Biol Cybern* 91(2):76–90
- Sponberg S, Full R (2008) Neuromechanical response of musculoskeletal structures in cockroaches during rapid running on rough terrain. *J Exp Biol* 211:433–446
- Sponberg S, Spence A, Mullens C, Full R (2011) A single muscle's multifunctional control potential of body dynamics for postural control and running. *Philos Trans Roy Soc B* 366:1592–1605
- Ting L, Blickhan R, Full R (1994) Dynamic and static stability in hexapedal runners. *J Exp Biol* 197:251–269
- Zill S, Moran D (1981a) The exoskeleton and insect proprioception I. Responses of tibial campaniform sensilla to external and muscle-generated force in the American cockroach *Periplaneta americana*. *J Exp Biol* 91:1–24
- Zill S, Moran D (1981b) The exoskeleton and insect proprioception III. Activity of tibial campaniform sensilla during walking in the American cockroach *Periplaneta americana*. *J Exp Biol* 94:57–75
- Zill S, Moran D, Varela F (1981) The exoskeleton and insect proprioception II. Reflex effects of tibial campaniform sensilla in the American cockroach *Periplaneta americana*. *J Exp Biol* 94:43–55